

PAPER

Magnetic flux instability in NbN films exposed to fast field sweep rates

To cite this article: E Baruch-El *et al* 2018 *Supercond. Sci. Technol.* **31** 105008

View the [article online](#) for updates and enhancements.



IOP | ebooks™

Bringing you innovative digital publishing with leading voices to create your essential collection of books in STEM research.

Start exploring the [collection](#) - download the first chapter of every title for free.

Magnetic flux instability in NbN films exposed to fast field sweep rates

E Baruch-Ei^{1,4} , M Baziljevich^{1,2}, T H Johansen², X Y Zhou³, X Q Jia³ , B B Jin³, A Shaulov¹ and Y Yeshurun¹

¹Institute of Superconductivity and Institute of Nanotechnology, Department of Physics, Bar-Ilan University, Ramat-Gan 5290002, Israel

²Department of Physics, University of Oslo, NO-0316 Oslo, Norway

³Research Institute of Superconductor Electronics (RISE), School of Electronic Science and Engineering, Nanjing University, Nanjing, 210093, People's Republic of China

E-mail: Elranbe@gmail.com

Received 12 July 2018, revised 5 August 2018

Accepted for publication 16 August 2018

Published 6 September 2018



CrossMark

Abstract

Magneto-optical imaging of dendritic flux instability is reported for NbN films exposed to magnetic fields ramped at a fast rate ($0.1\text{--}3.2\text{ kT s}^{-1}$). The results show that as the magnetic ramp rate increases, the temperature and field range of the instability extends significantly. In particular, the lower and upper threshold fields (H_1^{th} and H_2^{th} , respectively) that bound the field range for dendritic instability are affected. The upper field is found to increase linearly with the applied field sweep rate, a behavior which is discussed in terms of a recent theoretical work (Vestgarden *et al* 2016 *Phys. Rev. B* **73** 174511). The extended instability range should be taken into account in applications in which the superconducting films are exposed to rapid changes in the magnetic field.

Keywords: NbN, dendritic flux instability, magneto-optical imaging, superconductivity

(Some figures may appear in colour only in the online journal)

1. Introduction

Magnetic flux instability is quite common in type II superconductors, resulting in, for example, a suppression of the critical current density [1–4] and the generation of electromagnetic noise [5]. Such instability may limit applications of superconducting materials, and may even damage the material itself [6]. The instability occurs when vortices escape from pinning centers, locally heating the material, thus promoting additional flux motion and generating a positive feedback that results in large-scale flux avalanches. This phenomenon appears as flux jumps in wires and bulk superconductors [7–9], and as dendritic flux formations in thin films. The latter has been observed in a large number of superconductors important for practical applications, such as MgB₂ [10, 11], Nb [12, 13], YBCO [14], and NbN [15].

NbN is a promising material for superconducting practical devices due to, e.g., its relatively high critical current density j_c , relatively high critical temperature T_c for a conventional superconductor, and simplicity of film preparation.

Consequently, NbN films have been found suitable for use in superconducting devices such as single-photon detectors [16], microwave resonators [17], hot electron bolometers [18] and kinetic inductance detectors [19]. Yet the dendritic avalanches may limit the usefulness of NbN in such devices.

Magneto-optical imaging (MOI) studies of superconducting films exposed to perpendicular magnetic fields have shown that the dendritic flux avalanches occur only below a certain threshold temperature, $T_{\text{th}} < T_c$ [20]. Also, at a given temperature the instability is limited to a certain range of applied fields, between a lower and an upper threshold fields, H_1^{th} and H_2^{th} , respectively [21], i.e. a minimum applied field, H_1^{th} , is needed in order to trigger an instability. Yet, upon increasing the field above a certain value, H_2^{th} , the film re-enters a ‘stable region’ where flux penetrates the superconductor with a smooth front.

Previous MOI experiments on NbN films [21–23] have focused attention on the effect of the external magnetic field on the instability, ignoring possible influences of the magnetic field sweep rate. In those experiments, the magnetic field was ramped ‘slowly’, at a rate defined by the experimental device, typically $\sim 1\text{ mT s}^{-1}$. In the present work we present results of

⁴ Author to whom any correspondence should be addressed.

the first experimental study of the flux instability regime in NbN films exposed to rapid sweep rates of the external magnetic field. The MOI results reveal that rapid sweep rates increase dramatically the instability region, pushing the threshold temperature closer to T_c . Moreover, for a given temperature, the threshold fields are dramatically affected by the sweep rate. It is found that the instability generated by rapid sweep rates is triggered by lower fields. Furthermore, the upper threshold field above which stability is restored increases linearly with the applied sweep rate. The significant extension of the instability regime can be of primary importance when designing devices that may be exposed to rapidly changing magnetic fields.

2. Experimental

With the background vacuum kept below 8×10^{-6} Pa, 300 nm NbN films were fabricated on 10×10 mm² MgO (100) substrates at ambient temperature by DC magnetron sputtering [24]. To reduce the lattice mismatch and the strain in the film, a 30 nm thick pre-coat of Nb5N6 was used as a buffer layer [25]. The Nb target is 8 inch in diameter with 99.999% purity and the distance between the target and substrates is about 6 cm. The deposition took place in a gas mixture of N₂ and Ar at the total pressure of 2 mTorr with a ratio of 1:7. The optimized sputtering current is 1.50 A, with deposition rate at 1 ± 0.05 nm s⁻¹. For these films, the normal to superconductor transition temperature, T_c , is ~ 15.6 K. The films were cut to 5×5 mm² squares to fit our MOI system [26] and a 5 T Quantum Design MPMS magnetometer. The effective ramp rate of the MPMS is ~ 1 mT s⁻¹. The MOI system enables real-time imaging at rates up to 70 000 frames per seconds and provides a maximum applied field of 60 mT with slow and fast sweep rates of 0.2–2 mT s⁻¹, and 0.1–3.2 kT s⁻¹, respectively. The fast sweep rates are obtained by charging a high inductance storage coil and discharging it to a smaller inductance field coil. The rate can be controlled by controlling the voltage of a power supply. In addition, metallic components of the cryostat were replaced by nonmetallic ones in order to reduce eddy current. For more details see [26].

3. Results

In all the MOI experiments described below the NbN films were zero field cooled (ZFC) to a temperature below the transition temperature, T_c , and then exposed to different magnetic field values, from which it was ramped down back to zero at various rates. Experiments at slow ramping rates (0.2–2 mT s⁻¹) exhibit dendritic avalanches at low temperatures up to a threshold temperature $T_{th} = 5.3$ K, similar to that reported in [23]. Typical results are shown in figure 1(a), exhibiting a MOI after ZFC the film to 4.2 K, exposing it to 60 mT and then ramping the field down to zero at a rate of

2 mT s⁻¹. The figure shows dendritic avalanches, seen as black antflux invasion into the sample. Above T_{th} the flux penetrated smoothly into the films. A typical example is shown in the MOI of figure 1(b) measured above T_{th} , at 6.7 K, for a field sweep rate of 2 mT s⁻¹. At this temperature, the remnant field shows the expected ‘roof-top’ pattern [27, 28].

Applying fast sweep rates resulted in a dramatic increase in the threshold temperature, i.e., we were able to trigger the instability deep in the region previously considered as a ‘stable region’. For instance, figure 1(c) shows dendritic avalanches at 6.7 K after decreasing the field from 15 mT to 0 at a rate of 2.5 kT s⁻¹. For this applied field and sweep rate we were able to detect avalanches up to a temperature of 10.6 K, twice as the threshold temperature that was found in the slow rate measurements.

Next, we searched for the minimum threshold field needed to generate an avalanche at a constant temperature, for various sweep rates. At 4.3 K, we found that the minimum field value was 15 mT for a slow sweep rate of 2 mT s⁻¹. But for a fast sweep rate of 1 kT s⁻¹, even a low value of ~ 4 mT was sufficient to produce an instability. This result indicates that fast sweep rates lower the field H_1^{th} needed to trigger the avalanches. The exact dependence of H_1^{th} on \dot{H}_a could not be resolved because of limitations of our system to change magnetic field values below 4 mT at fast sweep rates.

Experiments were repeated at different temperatures and fields, varying the sweep rate up to 3.2 kT s⁻¹, searching for an upper field limit for the avalanches. For temperatures below 5.5 K, avalanches persist up to our maximal experimental field of 60 mT for any sweep rate. An upper threshold field was measurable above 5.5 K. In figure 2 we summarize the experimentally measured H_2^{th} at $T = 6$ K, as a function of the field sweep rate. The figure reveals a linear dependence of H_2^{th} on \dot{H}_a . A similar linear dependence was obtained for several temperatures between 5.5 and 7 K. Above 7 K the contrast in the MOI was too poor to allow for a full characterization.

4. Discussion

The origin of the dendritic instability has already been discussed in several papers, see e.g. [1–4]. In brief, it is a result of competition between heat and magnetic flux diffusion in the sample. Vortex instability is found in the temperature and field range in which the magnetic diffusion prevails. The ratio between the magnetic and thermal diffusion coefficients is determined by sample parameters such as thermal conductivity, heat transfer to the substrate, and the sample critical current density, j_c . The latter serves as a measure for the resistance of the system to flux entry and thus it is a key parameter of the sample magnetic stability. Our results clearly show an extended instability regime at fast sweep rates in both temperature and field regimes. Fast magnetic sweep rates induce large electric fields, resulting in heat dissipation by the normal-conducting electrons in the vicinity of the vortex and thus further increase the local heat [29]. As a result, the

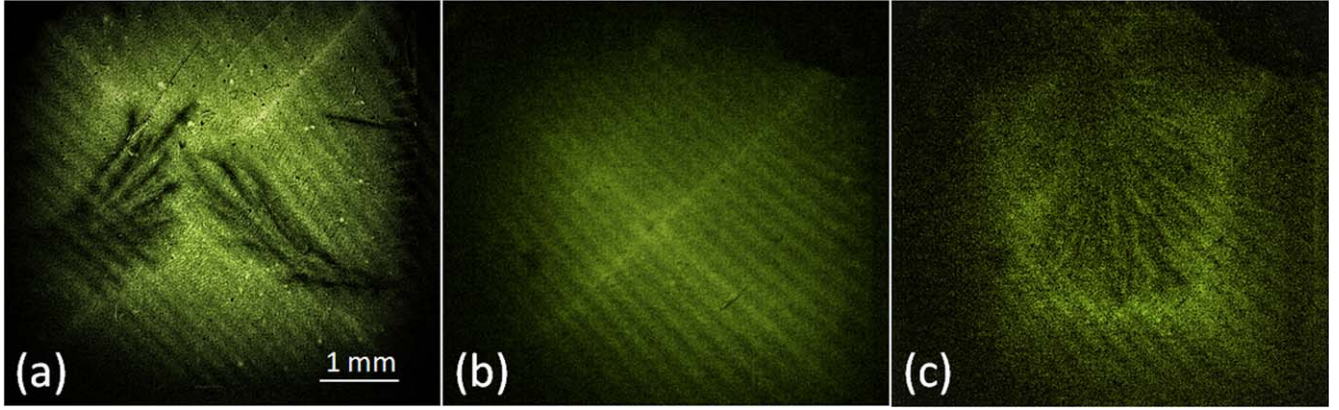


Figure 1. Magneto-optical imaging of the NbN film at different temperature and sweep rate conditions. The diagonal lines are interference fringes from the MOI indicator. (a) The film was ZFC to $T = 4.2$ K, a field $\mu_0 H_a = 60$ mT was applied at a slow ramp rate of 2 mT s^{-1} and then decreased back to zero at the same rate. The dendritic avalanches seen as antflux invasion into the sample. (b) $T = 6.7$ K, same thermal history and field sweep rate as in (a). A Bean ‘rooftop’ pattern of the remanent state indicates flux stability. (c) The film was ZFC to 6.7 K, a field of 15 mT was applied at a fast rate of 2.5 kT s^{-1} and then decreased to zero at the same rate.

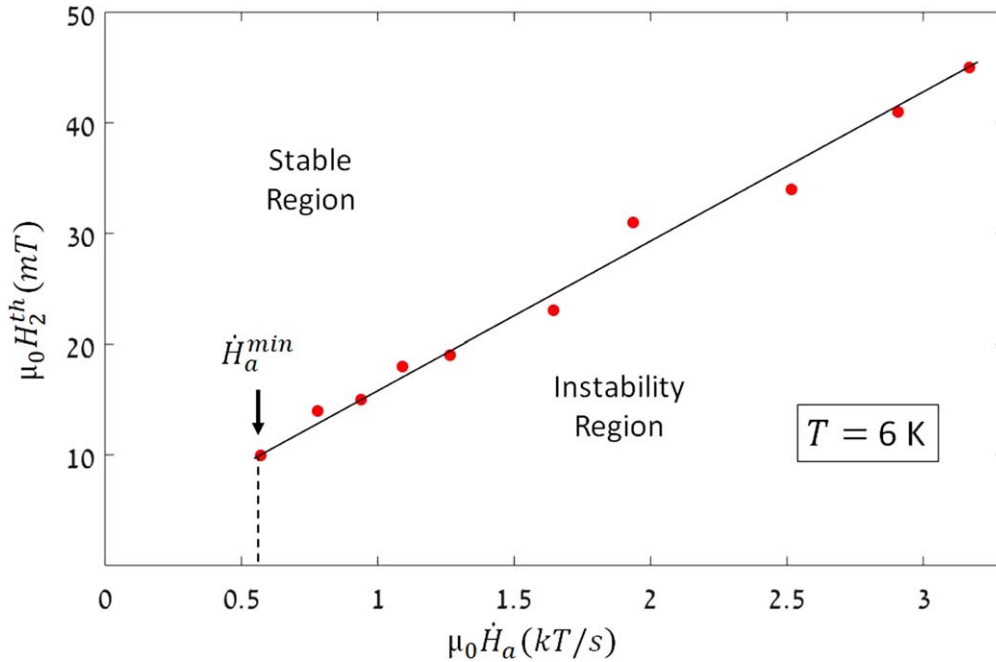


Figure 2. The upper threshold field as a function of the applied field sweep rate at 6 K. The solid line is a linear fit to the experimental data points. The arrow marks the minimum sweep rate below which the system is stable for any field.

instability is enhanced and the threshold temperature above which the instability vanishes is pushed up significantly, from 5.3 K for the slow sweep rates to ~ 10.6 K for the fast rates. A similar effect was seen in our previous study of MgB₂ films [10].

The main and new aspect of the present work is the experimental determination of the effect of \dot{H}_a on the threshold fields. Specifically, the results show indications for a decrease of the critical field H_1^{th} above which the instability appears and a linear increase of the threshold field H_2^{th} above which the stability is restored. These results can be explained on the basis of a recent theoretical study [30] of thermo-magnetic instability in superconducting films. This theory

predicts the following expression for the threshold magnetic field:

$$H_{th} = \frac{dj_c}{\pi} \operatorname{atanh} \left(\frac{hT^*}{nwdj_c \mu_0 \dot{H}_a} \right), \quad (1)$$

where d is the film thickness, j_c is the critical current density, h is the coefficient of heat transfer between the film and the substrate, $T^* = |\partial \ln j_c / \partial T|^{-1}$, n is the flux creep exponent, and w is the half-width of the film. Note that j_c depends on the external field, thus by inserting $j_c(H_a = H_{th})$ in equation (1), one obtains an equation for H_{th} for a given \dot{H}_a . As discussed below, equation (1) may yield two solutions—a lower and upper critical field, $H_1^{th}(\dot{H}_a)$ and $H_2^{th}(\dot{H}_a)$, respectively. Solving this equation

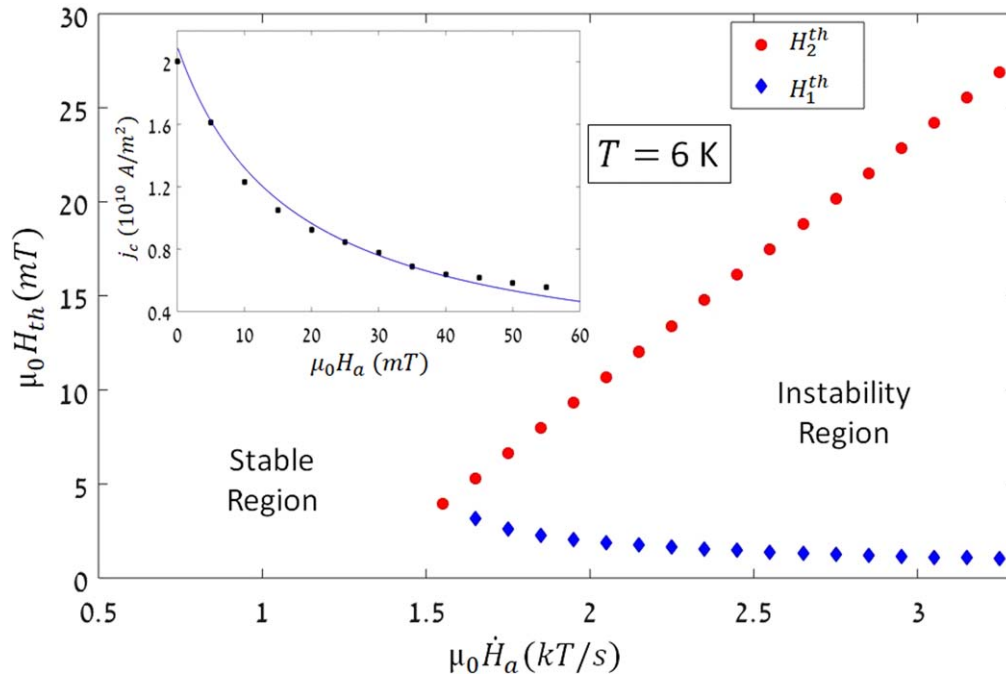


Figure 3. Numerical solution of the lower (diamonds) and upper (circles) threshold fields as a function of the applied sweep rate. Inset: field dependence of j_c at $T = 6$ K. The black squares represent experimental data points and the solid line is a fit according to the Kim critical current model, see text.

requires determination of the actual field dependence of j_c . To accomplish this task, we measured magnetic hysteresis loops (M versus H_a) for our NbN film (M is the film magnetization), using MPMS magnetometer after ZFC the film to various temperatures (between 2 and 10 K). $j_c(H_a)$ was determined from the width ΔM of the magnetization loops using $j_c = 30\Delta M/w$, where the pre-factor takes care of the geometry of our square film [28]. The inset to figure 3 shows the resulting j_c values (squares) as a function of the applied field at 6 K (same temperature as for the results displayed in figure 2). The solid line in the figure is a fit of the data to the Kim model [31]:

$$j_c = j_{c0}/(1 + H_a/H_0), \quad (2)$$

where $j_{c0} = 2.1 \times 10^{10} \text{ A m}^{-2}$ and $\mu_0 H_0 = 17 \text{ mT}$ (j_{c0} is the critical current density at zero field and H_0 is a sample-dependent characteristic field). Note that the critical current j_{c0} for our film is smaller by a factor of three to four as compared to values reported in the literature [21, 22]. This may explain the larger value of H_1^{th} at slow sweep rates in our measurements (15 mT) in comparison with previous experiments (2–5 mT in [22]).

As shown in [21, 22], under certain conditions equation (1) has two solutions representing the lower and upper threshold fields, H_1^{th} and H_2^{th} , respectively. The lower threshold field, H_1^{th} , is obtained for large j_c and it decreases as \dot{H}_a increases. The upper threshold field, H_2^{th} , is obtained for smaller j_c ; as j_c decreases the atanh term diverges, defining a threshold field above which the instability disappears. This field is obtained near the point where the argument of the atanh is approximately 1, i.e.

$$hT^*/(nwdj_c \mu_0 \dot{H}_a) \approx 1, \quad (3)$$

as the two curves representing both sides of equation (1) as a function of H_{th} must intersect at this point where the atanh diverges. Inserting j_c from equation (2) in (3) yields a linear relationship between H_2^{th} and \dot{H}_a the rate of change of the external field:

$$H_2^{th} = \frac{nwdj_{c0}\mu_0 H_0}{hT^*} \dot{H}_a - H_0. \quad (4)$$

The slope of this linear relationship can be determined experimentally from the data of figure 2, yielding $nwdj_{c0}\mu_0 H_0/hT^* = 13.5 \mu\text{s}^5$. Knowledge of this value allows numerical calculations of both the lower and upper threshold fields as a function of the field sweep rate, using equation (1). The results are shown in figure 3. The figure demonstrates the extension of the instability region; as the field sweep rate increases H_1^{th} (blue diamonds in the figure) decreases whereas H_2^{th} (red circles) increases. Most striking is the linear increase of H_2^{th} with \dot{H}_a that is confirmed experimentally, see figure 2. Also, the calculated and experimental H_2^{th} values are comparable. However, the experimental curve is shifted upward by approximately 20 mT. In other words, the experimental instability region is somewhat larger than expected theoretically, reflecting an excess local heating due to vortex/anti-vortex annihilation occurring at the edge of the film during field decrease [22, 23]. The calculated low values of the lower threshold field explain why we could not resolve

⁵ All the parameters in this expression are known experimentally ($w = 2.5 \text{ mm}$, $d = 300 \text{ nm}$, $\mu_0 H_0 = 17 \text{ mT}$, $j_{c0} = 2.1 \times 10^{10} \text{ A m}^{-2}$ and $T^* = |\partial \ln j_c / \partial T|^{-1} = 8.5 \text{ K}$), except for the n and the h . The measured slope implies $n/h = 4.3 \times 10^{-4} \text{ m}^2 \text{ K W}^{-1}$, a reasonable value which could mean, e.g., $n = 8$, $h = 1.8 \times 10^4 \text{ W m}^{-2} \text{ K}^{-1}$.

them experimentally at 6 K; as mentioned above, technical difficulties prevented us reaching such small threshold fields with high sweep rates. An experimental evidence for the decrease of H_1^{th} with \dot{H}_a is obtained at $T = 4.3$ K, where slow rates are sufficient to trigger the instability; we find experimentally that H_1^{th} decreases from 15 mT for a sweep rate of 1 mT s^{-1} , to 4 mT for 1 kT s^{-1} .

It is important to note that equation (1) is applicable only for \dot{H}_a values such that $hT^*/nwdj_c\mu_0\dot{H}_a \leq 1$. This dictates a minimum value of \dot{H}_a for the calculation of H_{th} given by $\dot{H}_a^{min} = hT^*/nwdj_c\mu_0$. Below this value, the system is stable for any applied field. The predicted value for \dot{H}_a^{min} at 6 K is 1.5 kT s^{-1} as shown in figure 3. This important prediction of a minimum sweep rate below which the system is stable is confirmed experimentally. However, the experimentally measured \dot{H}_a^{min} value at 6 K is 0.57 kT s^{-1} , see figure 2. As explained above, the experimental lower value of \dot{H}_a^{min} is because of the enhanced heating during the field decrease due to vortex/anti-vortex annihilation.

The new results regarding the extended instability region, are of concern to devices based on superconducting films exposed to rapid ramping magnetic fields or high-frequency AC fields. For example, NbN films used for shielding radiofrequency cavities for particle accelerators [32] are more prone to instability occurrence due to the exposure to high-frequency magnetic fields. The extended instability range is possibly a matter of concern also to applications using high electric fields and transient currents [33].

Based on our experimental results and those of others we propose possible ways of coping, at least partially, with the flux instability challenge. For example, our results suggest that the instability region may be bypassed by biasing the system to a large DC field. Also, a normal metal layer on top of the superconducting material [34, 35] may reduce the probability for an avalanche because of the eddy currents induced in the normal metallic layer. Of course, the efficiency of this solution should be investigated in the presence of a rapidly changing external field. Another parameter which may be important in bypassing the instability problem is the film substrate; as was demonstrated in [36], a proper choice of a substrate may reduce dramatically the problem by increasing the heat transfer from the film. Another solution may be based on previous findings of the strong dependence of the instability on the film thickness [37]. Apparently thicker films minimize the instability. This may be crucial for, e.g., NbN-based hot electron bolometers [18], as those are made of ultrathin films (usually a few nanometers) and thus may be found very prone to the magnetic instability.

In summary, this work presents the first experimental investigation of the flux instability boundaries in superconductors under fast sweep rates. NbN films, which are commonly used in various applications, were chosen for this study. We have found that fast field sweep rates affect the stability of the films, extending significantly the instability boundaries in terms of the threshold temperature and fields. In particular, the upper threshold field increases linearly as the magnetic field sweep rate increases, in agreement with recent

theoretical predictions. From practical point of view, all these results reveal that superconducting devices implementing high-frequency AC electromagnetic fields or transient currents are significantly more vulnerable to magnetic flux instability. All these results should be carefully considered in designing devices based on superconducting films.

Acknowledgments

This work was supported by Israel Science Foundation (ISF-164/12). The authors thank Lior Shani for technical assistance with the MPMS measurements.

ORCID iDs

E Baruch-El  <https://orcid.org/0000-0002-7300-9001>

X Q Jia  <https://orcid.org/0000-0002-4876-0370>

References

- [1] Mints R and Rakhmanov A 1981 Critical state stability in type-II superconductors and superconducting-normal-metal composites *Rev. Mod. Phys.* **53** 551
- [2] Denisov D V, Rakhmanov A L, Shantsev D V, Galperin Y M and Johansen T H 2006 Dendritic and uniform flux jumps in superconducting films *Phys. Rev. B* **73** 014512
- [3] Dvash E, Shapiro I and Shapiro B Y 2009 Dendritic instability of the magnetic flux in thermally anisotropic type-II superconductors *Phys. Rev. B* **80** 134522
- [4] Aranson I S, Gurevich A, Welling M S, Wijngaarden R J, Vlasko-Vlasov V K, Vinokur V M and Welp U 2005 Dendritic flux avalanches and nonlocal electrodynamics in thin superconducting films *Phys. Rev. Lett.* **94** 037002
- [5] Johansen T H, Baziljevich M, Shantsev D V, Goa P E, Kang W N, Kim H J, Choi E M, Kim M-S and Lee S I 2002 Dendritic magnetic instability in superconducting MgB₂ films *Europhys. Lett.* **59** 599
- [6] Baziljevich M, Baruch-El E, Johansen T H and Yeshurun Y 2014 Dendritic instability in YBCO films triggered by transient magnetic fields *Appl. Phys. Lett.* **105** 012602
- [7] Fujishiro H, Mochizuki H, Naito T, Ainslie M D and Giunchi G 2016 Flux jumps in high- J_c MgB₂ bulks during pulsed field magnetization *Supercond. Sci. Technol.* **29** 034006
- [8] Qureishy T, Laliena C, Martínez E, Qviller A J, Vestgården J I, Johansen T H, Navarro R and Mikheenko P 2017 Dendritic flux avalanches in a superconducting MgB₂ tape *Supercond. Sci. Technol.* **30** 125005
- [9] Pan A V, Zhou S, Liu H and Dou S 2003 Properties of superconducting MgB₂ wires: *in situ* versus *ex situ* reaction technique *Supercond. Sci. Technol.* **16** 639
- [10] Baruch-El E, Baziljevich M, Johansen T H, Albrecht J, Shaulov A and Yeshurun Y 2017 Dendritic flux instability in MgB₂ films above liquid hydrogen temperature *Supercond. Sci. Technol.* **31** 025005
- [11] Treiber S, Stahl C, Schütz G and Albrecht J 2011 Stability of the current-carrying state in nonhomogeneous MgB₂ films *Phys. Rev. B* **84** 094533

- [12] Vlasko-Vlasov V, Colauto F, Benseman T, Rosenmann D and Kwok W-K 2017 Guiding thermomagnetic avalanches with soft magnetic stripes *Phys. Rev. B* **96** 214510
- [13] Brisbois J, Motta M, Avila J I, Shaw G, Devillers T, Dempsey N M, Veerapandian S K, Colson P, Vanderheyden B and Vanderbemden P 2016 Imprinting superconducting vortex footsteps in a magnetic layer *Sci. Rep.* **6** 27159
- [14] Baruch-El E, Baziljevich M, Shapiro B Y, Johansen T H, Shaulov A and Yeshurun Y 2016 Dendritic flux instabilities in $\text{YBa}_2\text{Cu}_3\text{O}_{7-x}$ films: effects of temperature and magnetic field ramp rate *Phys. Rev. B* **94** 054509
- [15] Mikheenko P, Qureishy T, Mercier F, Jacquemin M and Pons M 2017 Dendritic flux avalanches in high-quality NbN superconducting films 2017 *IEEE 7th Int. Conf. Nanomaterials: Application and Properties (NAP)* (Piscataway, NJ: IEEE) p 02NTF05
- [16] Smirnov K, Divochiy A, Vakhtomin Y, Morozov P, Zolotov P, Antipov A and Seleznev V 2018 NbN single-photon detectors with saturated dependence of quantum efficiency *Supercond. Sci. Technol.* **31** 035011
- [17] Irimatsugawa T, Hirayama F, Yamamori H, Kohjiro S, Sato A, Nagasawa S, Fukuda D, Hidaka M, Sato Y and Ohno M 2017 Study of Nb and NbN resonators at 0.1 K for low-noise microwave SQUID multiplexers *IEEE Trans. Appl. Supercond.* **27** 1
- [18] Krause S, Meledin D, Desmaris V, Pavolotsky A, Rashid H and Belitsky V 2018 Noise and IF gain bandwidth of a balanced waveguide NbN/GaN hot electron bolometer mixer operating at 1.3 THz *IEEE Trans. Terahertz Sci. Technol.* **8** 365
- [19] Ariyoshi S, Nakajima K, Saito A, Taino T, Otani C, Yamada H, Ohshima S, Bae J and Tanaka S 2016 Terahertz response of NbN-based microwave kinetic inductance detectors with rewound spiral resonator *Supercond. Sci. Technol.* **29** 035012
- [20] Yurchenko V, Johansen T H and Galperin Y M 2009 Dendritic flux avalanches in superconducting films *Low Temp. Phys.* **35** 619
- [21] Yurchenko V, Shantsev D, Johansen T H, Nevala M, Maasilta I, Senapati K and Budhani R 2007 Reentrant stability of superconducting films and the vanishing of dendritic flux instability *Phys. Rev. B* **76** 092504
- [22] Qviller A, Yurchenko V, Eliassen K, Vestgården J, Johansen T H, Nevala M, Maasilta I, Senapati K and Budhani R 2010 Irreversibility of the threshold field for dendritic flux avalanches in superconductors *Physica C* **470** 897
- [23] Rudnev I A, Shantsev D V, Johansen T H and Primenko A E 2005 Avalanche-driven fractal flux distributions in NbN superconducting films *Appl. Phys. Lett.* **87** 042502
- [24] Kang L, Jin B, Liu X, Jia X, Chen J, Ji Z, Xu W, Wu P, Mi S and Pimenov A 2011 Suppression of superconductivity in epitaxial NbN ultrathin films *J. Appl. Phys.* **109** 033908
- [25] Jia X, Kang L, Gu M, Yang X, Chen C, Tu X, Jin B, Xu W, Chen J and Wu P 2014 Fabrication of a strain-induced high performance NbN ultrathin film by a Nb_5N_6 buffer layer on Si substrate *Supercond. Sci. Technol.* **27** 035010
- [26] Baziljevich M, Barness D, Sinvani M, Perel E, Shaulov A and Yeshurun Y 2012 Magneto-optical system for high speed real time imaging *Rev. Sci. Instrum.* **83** 083707
- [27] Polyanskii A, Gurevich A, Jiang J, Larbalestier D, Bud'ko S, Finnemore D, Lapertot G and Canfield P 2001 Magneto-optical studies of the uniform critical state in bulk MgB_2 *Supercond. Sci. Technol.* **14** 811
- [28] Gyorgy E, Van Dover R, Jackson K, Schneemeyer L and Waszczak J 1989 Anisotropic critical currents in $\text{Ba}_2\text{YCu}_3\text{O}_7$ analyzed using an extended Bean model *Appl. Phys. Lett.* **55** 283
- [29] Albrecht J, Matveev A, Djupmyr M, Schütz G, Stuhlhofer B and Habermeier H-U 2005 Bending of magnetic avalanches in MgB_2 thin films *Appl. Phys. Lett.* **87** 182501
- [30] Vestgården J I, Galperin Y and Johansen T H 2016 Oscillatory regimes of the thermomagnetic instability in superconducting films *Phys. Rev. B* **93** 174511
- [31] Kim Y, Hempstead C and Strnad A 1963 Magnetization and critical supercurrents *Phys. Rev.* **129** 528
- [32] Posen S, Transtrum M K, Catelani G, Liepe M U and Sethna J P 2015 Shielding superconductors with thin films as applied to rf cavities for particle accelerators *Phys. Rev. Appl.* **4** 044019
- [33] Bobyl A, Shantsev D, Johansen T H, Kang W, Kim H, Choi E and Lee S 2002 Current-induced dendritic magnetic instability in superconducting MgB_2 films *Appl. Phys. Lett.* **80** 4588
- [34] Colauto F, Choi E, Lee J, Lee S, Patiño E, Blamire M, Johansen T H and Ortiz W A 2010 Suppression of flux avalanches in superconducting films by electromagnetic braking *Appl. Phys. Lett.* **96** 092512
- [35] Mikheenko P, Vestgården J, Chaudhuri S, Maasilta I, Galperin Y and Johansen T H 2016 Metal frame as local protection of superconducting films from thermomagnetic avalanches *AIP Adv.* **6** 035304
- [36] Baruch-El E, Baziljevich M, Johansen T H and Yeshurun Y 2015 Substrate influence on dendritic flux instability in YBCO thin films *J. Supercond. Novel Magn.* **28** 379
- [37] Baruch-El E, Baziljevich M, Johansen T H, Shaulov A and Yeshurun Y 2018 Thickness dependence of dendritic flux avalanches in $\text{YBa}_2\text{Cu}_3\text{O}_{7-x}$ films *J. Phys.: Conf. Ser.* **969** 012042